REPORT TITLE:

ACTIVE CATHODES FOR SUPER-HIGH POWER DENSITY SOLID OXIDE FUEL CELLS THROUGH SPACE CHARGE EFFECTS

Reporting Period Start Date: July 1, 2004
Reporting Period End Date: September 30, 2004
Principal Author: Professor Anil V. Virkar
Date Report Was Issued: January 18, 2005
DOE Award Number: DE-FC26-02NT41602
Name and Address of Submitting Organization:

Department of Materials Science & Engineering
122 S. Central Campus Drive
University of Utah
Salt Lake City, UT 84112

DISCLAIMER:

ABSTRACT

This report summarizes the work done during the eighth quarter of the project. Effort was directed in two areas: (1) Development of a model of space charge and its application to porous bodies, with emphasis on the role of oxygen partial pressure. (2) Fabrication of porous samaria-doped ceria and the measurement of conductivity as a function of temperature and oxygen partial pressure.

TABLE OF CONTENTS

INTRODUCTION

Electrode transport properties, namely ionic and electronic conductivities, and morphology have a profound effect on electrode polarization and thus on solid oxide fuel cell (SOFC) performance [1-4]. A large part of the polarization loss is associated with the cathode in the form of activation polarization [5, 6]. In addition to the morphological effect, it is also known that the ionic conductivity of cathode has a large effect on cathodic polarization. This is expected to be the case regardless of whether the cathode is a mixed ionic electronic conducting (MIEC) composite cathode or a MIEC single-phase cathode. While the focus of the work discussed in this report is on composite cathodes such as LSM + YSZ, the general features are applicable to MIEC cathodes such as LSC, LSF, and LSCF. It is assumed that the electronic conductivity of the cathode is high enough, not to be a limiting factor. This is usually a good assumption with materials such as LSM and LSC, which have electronic conductivities over the temperature of interest between ~200 and 1000 S/cm. By contrast, the ionic conductivity of either YSZ or ceria or LSGM is well below 1 S/cm at similar temperatures. Even with the possible use of bismuth oxide for the cathode, the ionic conductivity is still much lower than the electronic conductivity of the electrocatalyst. The grain size also has a large effect on conductivity [7]. It is desired that the cathode microstructure close to the electrolyte be as fine as possible. When the particle size is very fine, there can be a significant effect of space charge on transport [8-13]. The effect of space charge can be potentially quite large in ionic conductors. It could either increase conductivity, or could decrease it. It is desired that the space charge be such that it enhances ionic conductivity of porous bodies. It is possible, however, that space charge effects are actually detrimental in many oxygen ion conductors. In such a case, the approach should be to seek to lower these effects. In the former case, it is desired that the cathodes be annealed at lower temperatures so as to increase the Debye length. In the latter case, it is desired that the cathodes be annealed at higher temperatures so as to suppress the Debye length. Work done to date suggests that in most materials of interest, the space charge tends to lower ionic conductivity. This implies that the cathodes need to be annealed at higher temperatures. The implication is that there are conflicting requirements from the standpoint of microstructural issues and space charge related issues, insofar as cathode polarization resistance is concerned.

One area in which space charge effects can be significant is the effect of grain size on conductivity, and especially of porous bodies. Another one of great importance is the morphology of the cathode, and especially that of the ionic conductor in composite cathodes. When ionic current has to flow from one grain to the adjacent grain, it is necessary that narrowing in the neck region be accounted for. In the past reports, preliminary results on both theoretical analysis and experimental aspects were reported. In this report, the possible effect of space charge on cathodic polarization is examined.

In this study, total conductivity of porous bodies including space charge effect and the role of oxygen partial pressure, was theoretically estimated. Also, in this study, the conductivity of porous SDC samples was measured as a function of oxygen partial pressure and temperature using a four-probe DC technique. The porous SDC samples used in this study were made by a three step method involving a leaching step. Then the

conductivity of the samples was measured using a four-probe DC technique at various temperatures and over a wide range in oxygen partial pressures.

EXECUTIVE SUMMARY

Solid oxide fuel cells (SOFC) can operate over a wide temperature range, from ~600 to 1000^{o}C, and can use a variety of hydrocarbon fuels, once appropriately processed. The current target for SOFC is about 800^{o}C, although efforts are presently underway to lower the operating temperature below 700^{o}C. The largest voltage loss (polarization) in SOFC is known to occur at the cathode, especially at relatively low temperatures (<800^{o}C). There are two types of cathodic polarizations: (1) Concentration polarization – that associated with gas transport. (2) Activation polarization – that associated with the occurrence of the overall electrochemical cathodic reaction of charge transfer. The former is relatively small, as long as the cathode is thin and has sufficient porosity [14]. The latter is the dominant one, and depends upon a number of microstructural and intrinsic – fundamental, parameters. This research aims to address cathodic activation polarization. Specifically, this research aims to lower the cathodic polarization by cathode modification through space charge effects. Our prior work has shown that the effective cathodic polarization resistance depends upon the following factors. (1) The particle size of the ionic conductor in a composite cathode, comprising a two phase, porous, contiguous mixture of an ionic conductor and an electrocatalyst – the latter being an electronic conductor. In general, the smaller the particle size of the ionic conductor, the lower is the cathodic activation polarization. (2) The ionic conductivity of the ionic conductor in the cathode also has a significant effect – the higher the ionic conductivity, the lower is the cathodic polarization. (3) Intrinsic charge transfer resistance – the lower the intrinsic charge transfer resistance, the lower is the cathodic activation polarization.

The above factors themselves depend upon additional fundamental parameters. It is known that in the majority of the ionic conductors, the smaller the grain size, the higher is the net resistivity. This is attributed to grain boundaries, which usually offer resistance to ion transport. Part of this resistance is attributable to space charge effect, which in some materials (e.g. YSZ) tends to lower oxygen vacancy concentration near grain boundaries. Depending upon the dopant type and amount, it is in principle possible to actually enhance the oxygen vacancy concentration near grain boundaries. If this can be achieved, significant lowering of cathodic polarization can occur. This research aims to identify fundamental parameters, which tend to increase oxygen vacancy concentration near grain boundaries. This is expected to depend upon the chemistry of the material as well as processing. In cases where the effect of space charge decreases ionic conductivity, a judicious choice of thermal treatment procedures may mitigate this detrimental effect.

The other factor involves the nature of inter-particle necks. If the contact between particles is narrow (small), the overall resistance can be large, leading to high cathodic polarization. During the previous reporting periods, the effect of inter-particle neck size on total conductivity of porous bodies was theoretically analyzed, and experimental results were presented. The results showed that the neck size between particles has a profound effect on ionic conductivity. Specifically, it was shown that for highly porous samples of identical porosities (~50%), the absolute value of conductivity was ~75 times higher in samples with sufficiently large neck sizes (good connectivity) as compared to samples with small neck sizes (poor connectivity). It is to be noted that this has profound influence on cathode

polarization. In the subsequent report (Third quarterly), the effect of grain boundaries was also included. However, the effect included was only that of the structural part of the grain boundary. It is known that the effect of space charge can extend far beyond the structural part of the grain boundary. In fourth quarterly report, results of further model development were included, wherein the effect of space charge region was explicitly included. Three cases have been considered: Space charge region having higher, equal to, and lower resistivity compared to the bulk grains. The effect of neck size on the effective resistivity has been explicitly calculated. In the seventh report, the space charge effects were explicitly included. Additionally, considerable work was done on the measurement of cell performance after subjecting the cells to thermal treatments so as to modify the Debye length, which should influence cathodic polarization. In earlier work, the role of oxygen partial pressure was ignored. However, in actual cell testing, the oxygen partial pressure can vary over wide range, depending upon the operating conditions, and whether ceria is used in the cathode, in the anode, or both. Hence, in the present work, the effect of oxygen partial pressure was examined, both theoretically and experimentally.

EXPERIMENTAL

During this reporting period, efforts were directed in the following areas.

1. Analysis of the effect of space charge on transport through porous bodies, and investigation of the role of oxygen partial pressure.

2. Fabrication of porous SDC samples.

3. Measurement of total conductivity as a function of temperature and oxygen partial pressure.

Detailed calculational and experimental procedures used are described below.

Modeling: Resistivity in Bulk and Space Charge Layer for Doped Ceria: In what follows, the role of space charge on total conductivity is examined. In the following discussion, all of the defects are assumed to be in thermodynamic equilibrium. Doped ceria is chosen here as a model material. Doped ceria is known [15-18] to be a mixed conductor of oxygen ions and electrons. Oxygen vacancies are created by introducing acceptor dopants by the reaction

$$A_2O_3 \rightarrow 2A^{'} + V_O^{\bullet\bullet} + 3O_O^{\times} \tag{1}$$

At elevated temperatures and at reduced oxygen partial pressures, electrons and oxygen vacancies can be generated by the following reaction, namely

$$O_O^{\times} \rightarrow 2e^{'} + V_O^{\bullet\bullet} + \frac{1}{2}O_2 \tag{2}$$

The corresponding law of mass action equation can be expressed as

$$n^2[V_O^{\bullet\bullet}] = k\exp(-\frac{\Delta H^o}{k_B T}) p_{O_2}{}^{-0.5} \tag{3}$$

where n is electron concentration, $\left[V_O^{\bullet\bullet}\right]$ is oxygen vacancy concentration, k is a constant, ΔH^o is the enthalpy of reaction (2), k_B the Boltzmann constant, and p_{O_2} is the oxygen partial pressure in ambient atmosphere.

According to the condition of local electro neutrality, the concentrations of $V_O^{\bullet\bullet}$ in the bulk can be expressed as:

$$[V_O^{\bullet\bullet}]_b = \frac{[A^{'}]_b + n}{2} \tag{4}$$

The dopant concentration in the bulk, $[A^{'}]_b$, p_{O_2} and temperature T are given by the experimental conditions. For cerium oxide, k = 1.2×10^{74} and ΔH^0 =4.67 eV [19]. From equation (3) and (4) the defect concentrations (oxygen vacancies and electrons) in the bulk can be calculated at various temperatures and oxygen partial pressures.

It is generally accepted that the total electrical conductivity for doped ceria is the sum of ionic conductivity and electronic conductivity.

$$\sigma = 2e[V_O^{\bullet\bullet}]\mu_{V_O^{\bullet\bullet}} + en\mu_e \tag{5}$$

Then the total conductivity in the bulk can be expressed as

$$\sigma_{bulk} = \sigma_{i(bulk)} + \sigma_{e(bulk)} = 2e[V_O^{\bullet\bullet}]_b \mu_{V_O^{\bullet\bullet}} + en_b\mu_e \tag{6}$$

where $[V_O^{\bullet\bullet}]_b$ & n_b are concentrations in the bulk in #/cm^3. $\mu_{V_O^{\bullet\bullet}}$ and μ_e are mobilities of oxygen vacancy and electron, respectively, in cm^2/volt.sec.

Then the resistivity in the bulk can be written as

$$\rho_b = \frac{1}{\sigma_b} = \frac{1}{2e[V_O^{\bullet\bullet}]_b \mu_{V_O^{\bullet\bullet}} + en_b\mu_e} \tag{7}$$

For ceria, the electron mobility is given by [19]

$$\mu_e(T) = \frac{3.9\times10^2}{T}\exp(-\frac{4.63\times10^3}{T}) \tag{8}$$

and the effective mobility of oxygen vacancies was given by [20]

$$\mu_{V_O^{\bullet\bullet}}(T) = \frac{2.92\times10^2}{T}\exp(-\frac{7.84\times10^3}{T}) \tag{9}$$

In the above analysis, constancy of the mobilities of oxygen vacancy and electrons was assumed. The assumption based on an ideal-solid-solution model that was utilized by Wang et al. [17] on the nonstoichiometry of doped ceria.

According to the constancy of the electrochemical potential for mobile defects, the concentration $n_j(x)$ of any dilute defect j with charge z in the space charge layer is given as

$$\frac{n_j(x)}{n_j(bulk)} = \exp[-z\frac{e\Delta\phi(x)}{kT}] \tag{10}$$

where x is the distance from the interface between the grain boundary core and the space charge layer, at the interface $x = 0$; $\Delta\phi(x)$ is the electrostatic potential referenced to the bulk, i.e., so called space charge potential. By solving Poisson's equation, it is related to the dopant concentration and space charge layer thickness by (for $x < \lambda^*$) [21]

$$\Delta\phi(x) = \frac{e[A^{'}]_b}{\varepsilon_0\varepsilon_r}\left(x-\lambda^*\right)^2 \tag{11}$$

where $[A^{'}]_b$ is the dopant concentration in the bulk in #/cm^3, ε_0 is permittivity of free space, space charge layer thickness λ^*, and Debye length λ can be given respectively by

$$\lambda^* = \lambda\sqrt{\frac{4e}{kT}\Delta\phi(0)} \text{ and } \lambda = \sqrt{\frac{kT\varepsilon_0\varepsilon_r}{4e^2[A^{'}]_b}} \tag{12}$$

where $\Delta\phi(0)$ is space charge potential at grain boundary. ε_r is the dielectric constant of material. For ceria ε_r = 26 [22]. The electron and oxygen vacancy concentrations in the space charge layer can be expressed respectively by

$$n_{(x)} = n_b \exp(\frac{q\Delta\phi(x)}{kT}) \tag{13}$$

and

$$[V_O^{\bullet\bullet}]_{(x)} = [V_O^{\bullet\bullet}]_b \exp(-\frac{2q\Delta\phi(x)}{kT}) \tag{14}$$

Then the specific conductivity in the space charge layer at a distance of x from grain boundary core is given as

$$\sigma_{sc(x)} = 2e[V_O^{\bullet\bullet}]_{(x)}\mu_{V_O^{\bullet\bullet}} + en_{(x)}\mu_e \tag{15}$$

The average electronic conductivity in the space charge layer can be given as

$$\sigma_{e(sc)} = \frac{1}{\frac{1}{\lambda^*}\int_0^{\lambda^*}\frac{1}{\sigma_e(x)}dx} \tag{16}$$

Inserting equations (11), (12) and (13) into equation (15) and rearranging

$$\sigma_{e(sc)} = \frac{e\mu_e n_b \lambda^*}{\int_0^{\lambda^*}\frac{1}{\exp[\frac{e^2[A^{'}]_b}{\varepsilon_0\varepsilon_r kT}\left(x-\lambda^*\right)^2]}dx} = \sigma_{e(bulk)}\frac{\lambda^*}{\int_0^{\lambda^*}\frac{1}{\exp[\frac{e^2[A^{'}]_b}{\varepsilon_0\varepsilon_r kT}\left(x-\lambda^*\right)^2]}dx} \tag{17}$$

Similarly, the average ionic conductivity in the space charge layer can be given as

$$\sigma_{i(sc)} = \frac{1}{\frac{1}{\lambda^*}\int_0^{\lambda^*}\frac{1}{\sigma_i(x)}dx} \tag{18}$$

Inserting equations (11), (12) and (13) into equation (18) and rearranging

$$\sigma_{i(sc)} = \frac{z_i e\mu_{V_O^{\bullet\bullet}}[V_O^{\bullet\bullet}]_b\lambda^*}{\int_0^{\lambda^*}\frac{1}{\exp[-\frac{z_i e^2[A^{'}]_b}{\varepsilon_0\varepsilon_r kT}\left(x-\lambda^*\right)^2]}dx} = \sigma_{i(bulk)}\frac{\lambda^*}{\int_0^{\lambda^*}\frac{1}{\exp[-\frac{z_i e^2[A^{'}]_b}{\varepsilon_0\varepsilon_r kT}\left(x-\lambda^*\right)^2]}dx} \tag{19}$$

Thus the average resistivity in the space charge region is then given by

$$\rho_{sc} = \frac{1}{\sigma_{sc}} = \frac{1}{\sigma_{e(sc)} + \sigma_{i(sc)}} \tag{20}$$

Fabrication and Conductivity Measurement of Porous Samaria Doped Ceria (SDC) Samples with Widely Varying Neck Sizes: Two different methods were used to make samples of various porosities. In the first method, powder compacts were formed by die-

pressing and iso-static pressing. Then the samples were sintered in air over a range of temperatures (ranging between 1200°C and 1600°C) to achieve varying porosity levels.

The process for making the second group of samples is as follows: Powder mixtures of commercial NiO and SDC (combustion method) in various NiO:SDC weight ratios corresponding to 20:80, 30:70 and 40:60 were wet-milled, dried, and then screened. Powder compacts were formed by die-pressing and iso-static pressing. Bar samples were sintered in air at 1600°C for 2 hours. The bar samples were then reduced in 10% hydrogen + 90% nitrogen gas mixture for 2 hours at 800°C, followed by a treatment in 100% hydrogen for 2 hours. Finally the reduced bar samples were leached in dilute nitric acid solution for 3 hours. This led to the removal of Ni as $Ni(NO_3)_2$, and created additional porosity. The resulting samples were single-phase, porous SDC.

Total conductivity of the two groups of samples of varying porosity levels was measured over a range of temperatures by four probe DC method. Prior to the measurement of conductivity, the samples were thermal treated at 1200°C for 4 hours to ensure the same space charge length among the samples. After testing, fractured pieces of each sample were impregnated with an epoxy. Upon curing and hardening the epoxy, the samples were mounted in plastic mount, and subsequently polished to a 1 micron finish. The samples were then examined under a scanning electron microscope (SEM). The microstructures of porous samples were characterized by quantitative stereology to estimate the porosity.

Conductivity Measurement of Porous SDC Sample at Various p_{O_2} & at Various Temperatures: Total conductivity of porous SDC samples fabricated using leaching process, was measured using four-probe DC technique in various p_{O_2} andat various temperatures. The p_{O_2} was changed from 1 atm (pure oxygen) to lower values, step by step, and finally to a reducing atmosphere. Oxygen partial pressure was controlled by N_2/O_2 mixtures for p_{O_2} higher than 10^{-5} atm, or H_2/H_2O mixtures for reducing atmospheres. The p_{O_2} was monitored using a oxygen sensor. After the measurement at 600°C, the sample was heated to higher temperatures to take new measurements.

RESULTS AND DISCUSSION

Oxygen Partial Pressure Effect on Effective Resistivity of Bulk and Space Charge Layer: Figure 1 shows the calculated defect concentrations (on a log scale) in the space charge layer as a function of distance from grain boundary core using the following parameters: T= 600°C, space charge potential = 0.4V [23], the doping level = 10% (corresponding to $n_b = 1.86\times10^{14}/cm^3$ and $\left[V_O^{\bullet\bullet}\right]_b = 1.34\times10^{21}/cm^3$). Note that in the space charge layer the oxygen vacancy concentration decreases and the electron concentration increases when approaching the grain boundary from the bulk. At grain boundary core, the oxygen vacancy concentration is still higher than that of electrons. For the case of T = 800°C, space charge potential = 0.4V, doping level = 10% as shown in Figure 2, note that the lines of oxygen vacancy concentration and electron concentration cross at ζ (distance

from grain boundary core) = 0.1 nm. When $\zeta < 0.1$ nm the so called "inversion layer" is formed. If the inversion layer is dominant in the space charge layer, the phenomenon of the space charge layer conductivity being higher than that of the bulk will be observed.

Figure 3 shows the calculated ionic, electronic and total conductivity (ionic plus electronic) in the bulk and the space charge layer as a function of various oxygen partial pressures using the following parameters: T = 600°C, space charge potential = 0.4V, doping level = 10 mol%. Note that in the bulk and in the space charge layer, the electronic conductivity increases about 3 to 4 orders magnitude when the p_{O_2} decreases from 1 atm to 10^{-15} atm. However the ionic conductivity for all cases remains independent of p_{O_2}. Also the ionic conductivity dominates the total conductivity over the whole p_{O_2} range.

Figure 4 shows the calculated ionic, electronic and total conductivity (ionic plus electronic) in the bulk and the space charge layer as a function of oxygen partial pressures using the following parameters: T = 800°C, space charge potential = 0.4 V, doping level = 10 mol%. It is seen that the average electronic conductivity in the space charge layer dominates the average total conductivity when $p_{O_2} < 10^{-7.6}$ range, which is in good agreement with expectation. At a higher temperature, the electron concentration can be larger at low p_{O_2}, thus the space charge layer exhibits lower resistivity than the bulk.

Figure 5 shows the calculated effective conductivity of porous doped ceria as a function of oxygen partial pressure at various temperatures for the case of grain size = 2.5 μm, theta = 18° (an indicator of relative neck size) and porosity = 30%. It is seen that at 600°C the conductivity remains constant with p_{O_2}. This can be attributed to the dominant ionic conductivity which is nearly constant over a wide range of p_{O_2}. However the effective conductivity increases from 0.02 S/cm to 0.033 S/cm with the decrease of p_{O_2} from 1 atm to 10^{-15} atm, which shows the effect of p_{O_2} on the effective conductivity. Figure 6 shows the measured effective conductivity of porous doped ceria as a function of oxygen partial pressure at various temperatures. The result shows similar trend with the previous simulation results. Thus the increase of electrical conductivity with reducing oxygen partial pressure can be explained by the space charge model.

CONCLUSION

An analytical equation to describe the conductivity of porous bodies, which incorporates the effects of the structural part of the grain boundary, the effect of space charge, and the relative neck size between contacting particles, was derived. Using calculated values of parameters, the effect of grain size and neck size on transport properties of porous ionic conductors was evaluated. The results show that a small neck size has a profoundly adverse effect on conductivity. The space charge layer in the grain boundary regions and

free surfaces in porous bodies also has a significant effect on the effective conductivity. Oxygen partial pressure effect on effective resistivity of bulk and space charge layer was evaluated. By comparing calculated and measured effective conductivities of porous doped ceria as a function of oxygen partial pressure at various temperatures, it was concluded that the increase of electrical conductivity with reducing oxygen partial pressure can be explained very well by defect chemistry and the space charge model. The simulation results also show that the ionic conductivity can influence the electrode polarization of composite electrode.

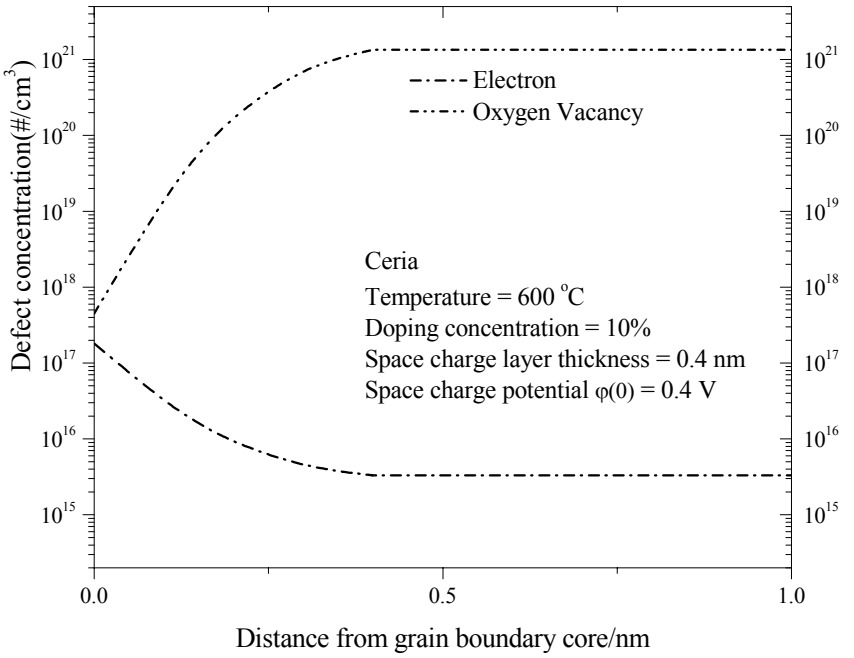

Figure 1: Calculated defect concentrations (on a log scale) in the space charge layer as a function of distance from the grain boundary core at 600°C.

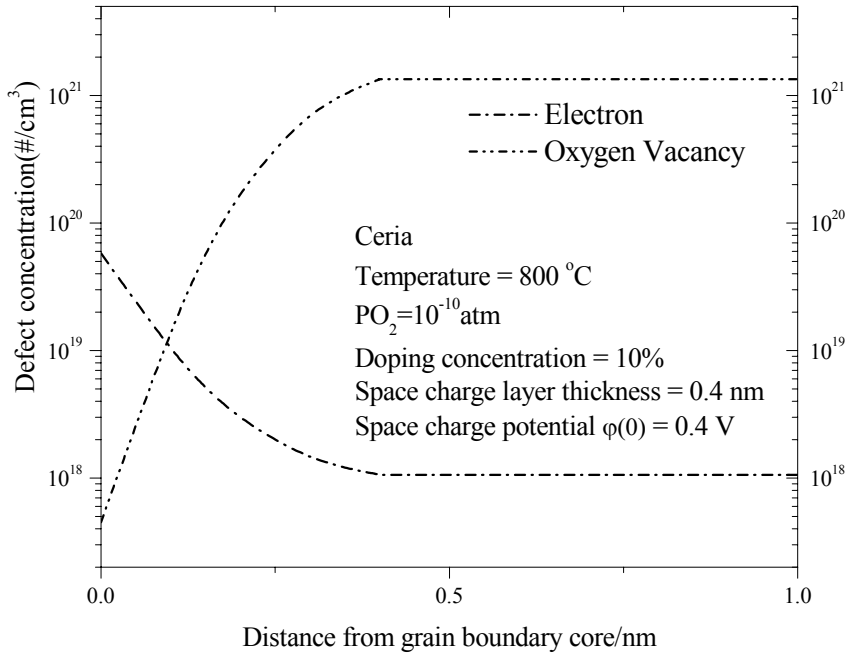

Figure 2: Calculated defect concentrations (on a log scale) in the space charge layer as a function of distance from the grain boundary core at 800°C.

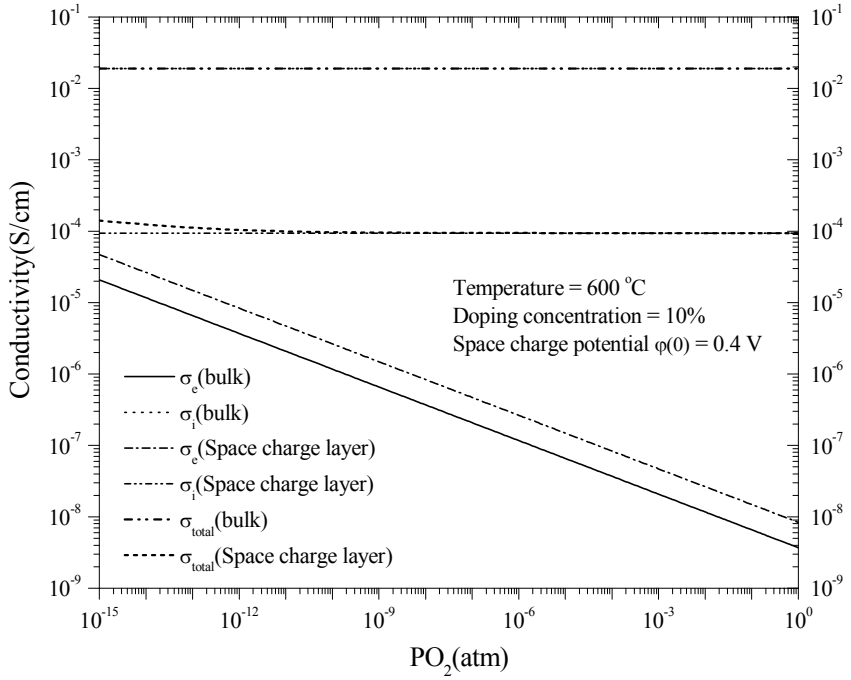

Figure 3: Calculated ionic, electronic conductivity and total conductivity (on a log scale) in bulk and space charge layer as a function of oxygen partial pressure.

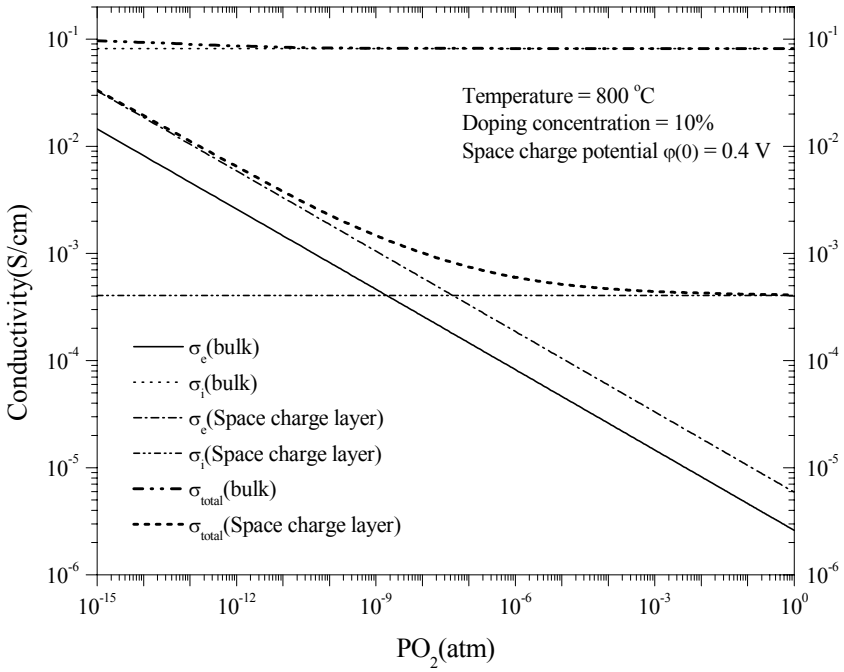

Figure 4: Calculated ionic, electronic conductivity and total conductivity (on a log scale) in bulk and space charge layer as a function of oxygen partial pressure.

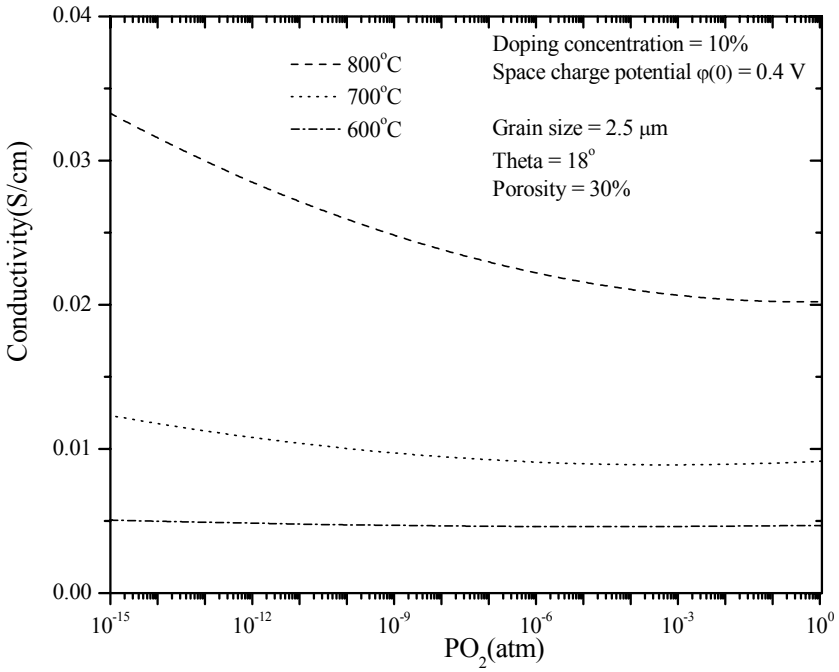

Figure 5: Calculated ionic and electronic conductivities (on a log scale) as a function of oxygen partial pressure.

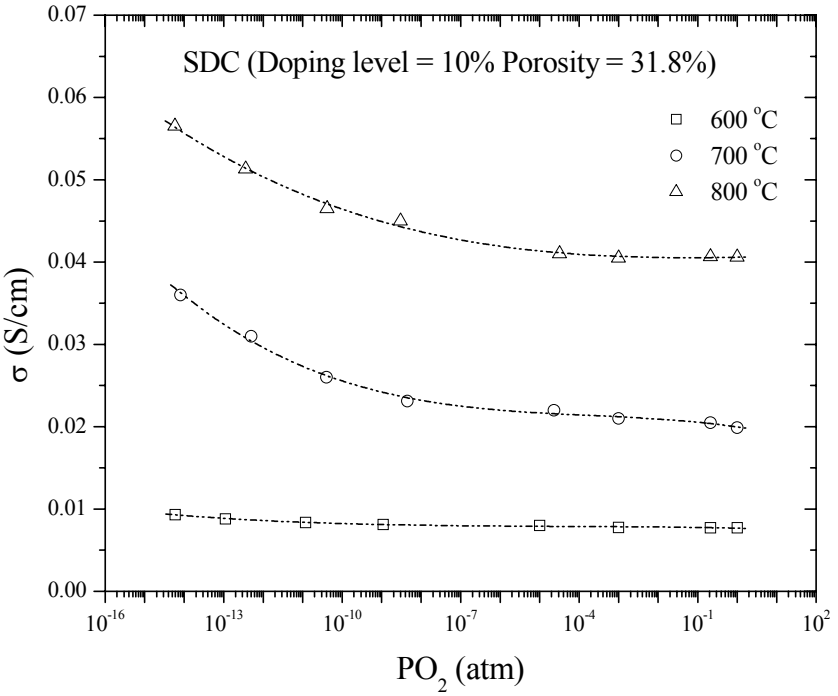

Figure 6: Measured total electrical conductivity (on a log scale) by 4-probe technique as a function of oxygen partial pressure.

REFERENCES

1) T. Kenjo, S. Osawa, and K. Fujikawa, *J. Electrochem. Soc*., **138** 349 (1991).
2) C. W. Tanner, K-Z. Fung, and A. V. Virkar, *J. Electrochem. Soc*., **144** 21-30 (1997).
3) H. Deng, M. Zhou, and B. Abeles, *Solid State Ionics*, **74** 75 (1994).
4) I. V. Murygin, *Elektrokhimiya*, **23** [6] 740 (1987).
5) A. V. Virkar, J. Chen, C. W. Tanner, and J-W. Kim, *Solid State Ionics*, **131** 189 (2000).
6) F. Zhao, Y. Jiang, G-Y. Lin, and A. V. Virkar, pp. 501 in SOFC VII, edited by H. Yokokawa and S. C. Singhal, Electrochemical Society Publication, Pennington, NJ, (2001).
7) M. J. Verkerk, B. J. Middlehuis, and A. J. Burggraaf, *Solid State Ionics*, **6** 159 (1982).
8) X. Guo, *Solid State Ionics*, **81** 235-242 (1995).
9) X. Guo, *Solid State Ionics*, **99** 137-142 (1997).
10) J. Frenkel, p. 37 in 'Kinetic Theory of Liquids', Dover, NY (1946).
11) K. Lehovec, *J. Chem. Phys*., **21** [7] 1123-1128 (1953).
12) K. L. Kliewer and J. S. Koehler, *Phys. Rev*., **140** [4A], A1226-A1240 (1965).
13) K. L. Kliewer, *Phys. Rev*., **140** [4A], A1241-A1246 (1965).
14) F. Zhao, T. Armstrong, and A. V. Virkar, *J. Electrochem. Soc*., **150** [3] A249-A256 (2003).
15) H. L. Tuller and A. S. Nowick, *J. Electrochem. Soc.*, 126, **209** (1979).
16) D. Scheider, M. Gödickemeier, and L. J. Gauckler, *J. Electroceram.*, 1, **165** (1997).
17) D. Y. Wang and A. S. Nowick, *J. Solid State Chem.*, 35, **325**(1980).
18) R. Gerhardt and A. S. Nowick, *J. Am. Ceram. Soc.*, **69**, 641(1986).
19) H.L. Tuller, in Nonstoichiometric Oxides, edited by T. O. Sørensen (Academic Press, New York, 1981), P. 271.
20) S. Wang, T. Kobayashi, M. Dokiya and T. Hashimoto, *J. Electrochem. Soc.*, **147** (10), 3906-09 (2000).
21) X. Guo and J. Maier, *J. Electrochem. Soc*., **148** [3] E121-E126 (2001).
22) D. Y. Wang, D. S. Park, J. Griffith and A. S. Nowick, *Solid State Ionics*, **2**, 95 (1981).
23) X. Guo, W. Sigle and J. Maier, *J. Am. Ceram. Soc.*, **86**, 77-87(1987).

LIST OF ACRONYMS AND ABBREVIATIONS

DC:	Direct current
LSC:	Sr-doped $LaCoO_3$
LSCF:	Sr-doped $La(Co,Fe)O_3$
LSGM:	Sr- and Mg-doped $LaGaO_3$
LSM:	Sr-doped $LaMnO_3$
MIEC:	Mixed ionic and electronic conduction or conductor
SDC:	Samaria-Doped Ceria
SOFC:	Solid oxide fuel cell
YSZ:	Yttria-stabilized zirconia